JOURNAL OF AIRCRAFT
Vol. 41, No. 2, March–April 2004

Wake Displacement Modifications to Reduce Rotorcraft Blade–Vortex Interaction Noise

Juan C. Abelló* and Albert R. George†
Cornell University, Ithaca, New York 14853-7501

Increasing the vertical separation between the rotor and its wake can reduce the strength of blade-vortex interaction (BVI) noise. A simple, first-order analytical model is developed to estimate the vertical distance between the rotor and the wake at any location of interest in the rotor disk. This model is used as an indicator to evaluate the potential effects of added forces, descent angle, advance ratio, and thrust coefficient on the separation between the wake and the rotor with the aim of identifying strategies that maximize this distance at a particular rotor disk location. The analysis focuses on landing approaches for helicopters and tiltrotors operating near helicopter configuration. The most appropriate strategies to increase this separation at the location of interest are found to depend on whether the wake is initially above or below the rotor. Added drag, added downforce, shallower descents, lower advance ratios, and higher thrust coefficients are shown to be desirable if the wake is initially below the rotor plane at the location of interest; this is the case of tiltrotor approaches and some helicopter descent operations. On the other hand, added thrust, added lift, steeper descents, higher advance ratios, and lower thrust coefficients are usually more appropriate if the wake is initially above the rotor plane at the location of interest; this is the case for other helicopter descent operations.

Nomenclature

A	=	rotor disk area
AR	=	tiltrotor wing aspect ratio
$C_{D_{i,w}}$	=	tiltrotor wing-induced drag coefficient
$C_{D_{\text{other}}}$	=	tiltrotor drag coefficient accounting for total parasite drag, tail-induced drag, and any fuselage- and nacelle-induced drag
$Cl_{\max}$	=	maximum wing lift coefficient
C_T	=	thrust coefficient
D	=	total tiltrotor drag accounting for all parasite and induced drag
D_f	=	helicopter fuselage drag
DL	=	rotor disk loading, T/A
e	=	Oswald efficiency factor
F_x	=	added x force, negative for added drag, positive for added thrust
F_z	=	added z force, negative for added downforce, positive for added lift
$F_{z\,\max}$	=	maximum added z force
f_e	=	equivalent flat plate area
g	=	gravitational acceleration
H	=	rotor H force
I_n	=	tiltrotor nacelle angle, measured from the fuselage waterline to the nacelle axis, 0 deg for airplane mode, 90 deg for helicopter mode
i_w	=	tiltrotor wing incidence angle, measured from the fuselage waterline to the wing zero lift line
k_x	=	induced inflow weighting factor along the X direction
k_y	=	induced inflow weighting factor along the Y direction
L	=	total tiltrotor lift accounting for wing, tail, and fuselage lift
m	=	rotorcraft mass
q	=	dynamic pressure, $\frac{1}{2}\rho v^2$
R	=	rotor radius
S	=	wing area
T	=	rotor thrust
v	=	flight speed
v_{tip}	=	blade tip speed
W	=	rotorcraft weight
X, Y, Z	=	longitudinal, lateral, and vertical rotor disk plane axes, normalized by rotor radius
X_0	=	initial X location of a fluid particle, normalized by rotor radius
x, z	=	longitudinal and vertical wind axes
Z_w	=	approximate vertical wake displacement normalized by rotor radius, positive upwards
α_{TPP}	=	tip path plane (TPP) angle of attack, negative nose down
α_w	=	tiltrotor wing angle of attack
Γ	=	incoming vortex circulation
γ	=	glideslope angle, positive for climb and negative for descent
ΔD	=	change in tiltrotor induced drag due to an added z force
ΔL	=	change in tiltrotor lift due to an added x force
$\Delta\alpha_{\text{TPP}}$	=	change in tip path plane angle of attack, final α_{TPP} minus initial α_{TPP}
$\Delta\gamma$	=	change in glideslope angle, final γ minus initial γ
Θ	=	tiltrotor fuselage pitch angle
λ	=	nondimensional rotor inflow
λ_i	=	nondimensional induced rotor inflow
$\lambda_{i,0}$	=	uniform nondimensional induced rotor inflow
μ	=	rotor advance ratio, $v\cos(\alpha_{\text{TPP}})/v_{\text{tip}}$
ρ	=	air density
χ	=	wake skew angle
Ψ	=	blade azimuth angle

Presented as Paper 99-1931 at the AIAA/CEAS 5th Aeroacoustics Conference, Bellevue, Washington, 10–11 May 1999; received 9 May 2001; revision received 1 April 2003; accepted for publication 4 April 2003.

*Graduate Research Assistant, Sibley School of Mechanical and Aerospace Engineering. Student Member AIAA.

†Carr Professor of Mechanical and Aerospace Engineering, Sibley School of Mechanical and Aerospace Engineering. Fellow AIAA.

Introduction

ONE of the main factors that currently limit the success of helicopters and tiltrotors is the noise level they can generate. Several components of a rotorcraft may contribute to its overall acoustic signature, and the noise generated by each of these may appear due

to different source mechanisms. The relative importance of these sources depends on the rotorcraft operating conditions; hence the appropriate noise reduction strategy can vary widely across the flight envelope and rotorcraft noise reduction can become a complicated task. For general reviews of rotorcraft noise, see Refs. 1 and 2.

Rotor noise mechanisms are often divided into three classes.

1) High-speed impulsive (HSI) noise, which is due to high Mach number advancing blades in high-speed forward flight. HSI noise is heard far in front of the rotorcraft.

2) Broadband noise, which is caused by random blade loading fluctuations due to self-induced or inflow turbulence. This type of noise can be important in local airport or heliport operations.

3) Blade–vortex interaction (BVI) noise, which appears from the rapid blade loading fluctuations occurring when a rotor blade has a close interaction with a trailing vortex generated by the previous passage of a rotor blade through the same air. BVI noise is radiated generally downward and usually dominates other noise sources when it occurs: during most landing descent approach conditions.

The present study focuses on BVI noise reduction for helicopter and tiltrotor aircraft through certain changes in rotorcraft design or flight operations. Because most of these changes will cause performance penalties, their implementation is considered only during those parts of the flight operations where noise reduction is needed, particularly during landing approach near populated areas.

A schematic view of a two-dimensional interaction between a blade and a vortex is shown in Fig. 1. The noise caused by this interaction depends on the following four parameters.

1) The first parameter is the incoming vortex circulation Γ.

2) The second parameter is the incoming vortex core structure. This has an effect only in cases where the blade actually intersects the vortex core. Note that these first two parameters are set by the circulation and geometry of the previous blade passage that generated the vortex.

3) The third parameter is the miss distance. Miss distance can be defined (somewhat arbitrarily) as the distance existing between a particular vortex segment and the quarter-chord line of a particular blade section, measured perpendicular to the local oncoming flow velocity. For a given vortex strength, the miss distance determines the disturbance velocity seen at the blade; increasing miss distance decreases this disturbance velocity and the resulting BVI noise. Note that the sound pressure is proportional to the time rate of change of local blade loading. Therefore, the sound pressure decreases with increasing miss distance due to both the decreased disturbance strength and the stretched timescale associated with a larger miss distance. (If existing, active modification of the airfoil response may change the blade load fluctuations and could be considered. Active airfoil response can be achieved by employing active flaps, active blade twist, etc.[3])

4) Finally, if one considers the top view of the three-dimensional BVI geometry projected onto the rotor plane (Fig. 2 from Ref. 4), one can see another factor that affects BVI noise strength: the geometry

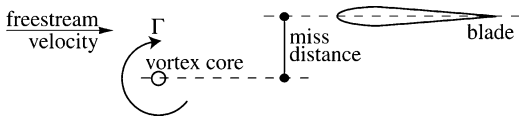

Fig. 1 BVI schematic.

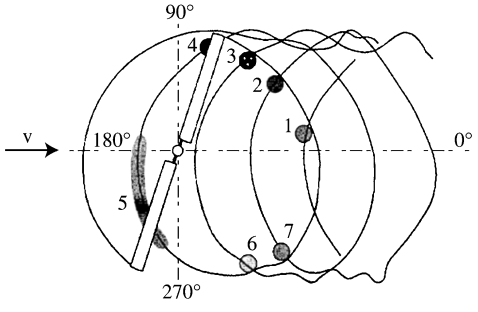

Fig. 2 Top view of BVI geometry, from Ref. 4.

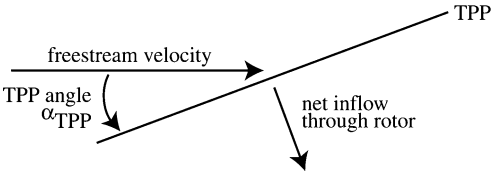

Fig. 3 Rotor inflow schematic; TPP angle shown negative.

of the interaction. In a two dimensional top view, the rotor advance ratio sets the interaction geometry, its angle variation, and the path of the interaction relative to the fluid. The resulting velocity of the interaction relative to the fluid determines the varying trace Mach number of the load fluctuation and thus its radiation.[5] If the corresponding trace Mach number is transonic or supersonic, the interaction radiates much more strongly and directionally than if it is subsonic.[5]

The interaction geometry will change with variations in forward flight velocity (hence advance ratio). The resulting changes in trace Mach number effects are not analyzed in the present paper, but are known to have large effects on BVI strength and directionality.[6–8]

This paper is primarily concerned with miss distance (the third parameter). For the purposes of this study, miss distance is considered as the vertical distance between the rotor plane and the mean vortex wake at a given location in the rotor plane. The miss distance is strongly dependent on rotor inflow, which in turn is highly nonuniform across the rotor disk. As a consequence, miss distance usually varies between different BVI events and, for a given event, it may also change in time as the blade and vortex line move in space.

The purpose of the present study is to determine how different trim parameters and rotorcraft flight conditions affect the vertical displacement of the wake relative to the rotor plane and thus BVI. Because the rotor inflow is nonuniform across the rotor disk, the vertical wake displacement is estimated at a particular point in the rotor plane where strong BVI is known to occur. The vertical wake displacement thus obtained provides an approximation for the miss distance at the given location in the rotor plane; this simplified view allows the identification of trim parameters that tend to increase the separation between the mean wake and the rotor plane and hence reduce BVI levels.

Starting from the inflow model presented in the following section, a model is developed to calculate the approximate vertical wake displacement Z_w at any location in the rotor plane. Simple trim models for helicopter and tiltrotors are then presented, and expressions relating rotor tip path plane angle α_{TPP} (Fig. 3) to added forces and flight parameters are derived in closed form.

The trim models and the approximate vertical wake displacement model are then used to study the effects of added forces, descent angle, advance ratio, and thrust coefficient on Z_w. Both added longitudinal and vertical forces are considered, and illustrations for helicopters and tiltrotors are presented and compared. Finally, existing experimental BVI noise data are employed to evaluate the usefulness of Z_w as a general indicator in BVI noise trends.

The idea of using added longitudinal forces (drag and thrust) or rotorcraft acceleration to modify BVI was first presented by Schmitz.[9] Controlling airframe lift vs rotor lift to reduce noise for tiltrotors has been considered in many studies of tiltrotor noise.[10] Glide path slope effects on rotorcraft BVI have also been investigated, although it is usually considered that the approach speed and glideslope angle are set by regulatory considerations.[11,12]

Preliminary results of the present research may be found in Refs. 13 and 14.

Inflow Model

Because miss distance is primarily given by the net inflow through the rotor, it is useful to better understand the dependence of rotor inflow on different rotorcraft parameters. Classic momentum theory in forward flight indicates the mean inflow through the rotor is a function of flight velocity (advance ratio), disk loading and air density (thrust coefficient), and inclination of the rotor tip path plane (TPP) with respect to the freestream velocity (TPP angle α_{TPP}). This dependence can be better seen in Fig. 3 and Eq. (1).

After nondimensionalizing the mean inflow velocity by the blade tip speed, the nondimensional mean rotor inflow λ can be related to the advance ratio μ, the thrust coefficient C_T, and the TPP angle α_{TPP} by the following expression:

$$\lambda = \lambda_i - \mu \tan(\alpha_{\text{TPP}}) \tag{1}$$

The first term on the right-hand side of Eq. (1) represents the induced inflow arising from thrust generation, whereas the second term appears due to the inclination of the rotor with respect to the freestream velocity. The $\mu \tan(\alpha_{\text{TPP}})$ term is straightforward to calculate, whereas more careful considerations must be made when modeling the induced inflow λ_i.

In the lowest level of approximation, the induced inflow λ_i can be modeled as uniform across the rotor disk. Under the uniform inflow assumption, Eq. (1) becomes

$$\lambda = \lambda_{i,0} - \mu \tan(\alpha_{\text{TPP}}) = \left[C_T \Big/ \left(2\sqrt{\mu^2 + \lambda^2}\right)\right] - \mu \tan(\alpha_{\text{TPP}}) \tag{2}$$

where $\lambda_{i,0}$ is the uniform inflow resulting from classic momentum theory.

The uniform induced inflow model presented in expression (2) is useful to gain insight into the dependence of λ on μ, C_T, and α_{TPP}. However, the induced inflow is not uniform under actual forward flight conditions; experimental observations indicate λ_i tends to be heavily biased toward the rear of the disk and weakly biased toward the retreating side.[15] Therefore, a higher level of refinement is desired if one wishes to better capture the general behavior of the miss distance at a particular location in the rotor plane.

A second level of approximation to the rotor inflow introduces corrections to $\lambda_{i,0}$ to better model the general variation of the induced inflow across the rotor plane; these formulations capture the general variation of λ_i over the rotor disk while being simple to implement and study. Most of these inflow models introduce weighting factors k_x and k_y to represent the variation of λ_i over the rotor plane, as shown in Eq. (3) (Ref. 15):

$$\lambda_i = \lambda_{i,0}(1 + k_x X + k_y Y) \tag{3}$$

where X and Y are the longitudinal and lateral coordinates along the rotor disk normalized by rotor radius (Fig. 4). X is positive downstream, Y is positive toward the advancing side, and their origin is at the rotor hub.

Several researchers have proposed different methods for finding suitable values for k_x and k_y. The analysis in this paper employs the weighting factors proposed by Drees[16] because they account for the inflow variation in both X and Y and have been found to yield one of the inflow models that best represents the overall inflow characteristics when compared to experimental measurements.[15] Note that this model was derived for helicopter rotors, and thus it may not fully capture the inflow variations of tiltrotors due to their highly twisted blades and higher disk loadings. If desired, other inflow models could naturally be used in Eq. (3); see Ref. 15 for an overview of possible alternatives.

The weighting factors k_x and k_y proposed by Drees are as follows[16]:

$$k_x = \frac{4}{3}\frac{1 - \cos(\chi) - 1.8\mu^2}{\sin(\chi)} \tag{4}$$

$$k_y = -2\mu \tag{5}$$

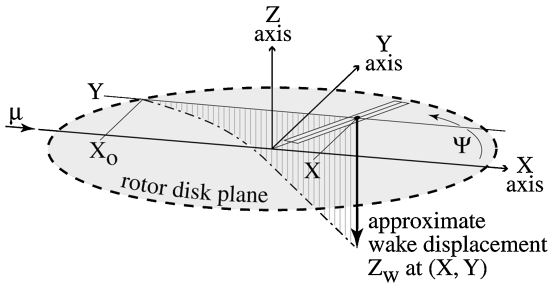

Fig. 4 Schematic of the approximate vertical wake displacement Z_w at a point (X, Y).

where χ is the wake skew angle given by

$$\chi = \arctan\{\mu/[\lambda_{i,0} - \mu \tan(\alpha_{\text{TPP}})]\} \tag{6}$$

Recall that the advance ratio μ is defined as $v\cos(\alpha_{\text{TPP}})/v_{\text{tip}}$ throughout this paper, where v_{tip} is the blade tip speed.

The miss distance depends on the net rotor inflow, with near-zero inflow conditions corresponding to small miss distances and hence high BVI noise likelihood.[2] Therefore, the miss distance can be expected to depend on μ, α_{TPP}, and C_T for a given (X, Y) location in the rotor plane as illustrated by expressions (1–3).

For low forward flight speeds where the advance ratio is small compared to the nondimensional hover-induced velocity $\sqrt{(C_T/2)}$, the first term in Eq. (1) becomes important when compared to the second. This implies the mean rotor inflow and hence the average miss distance is mostly dependent on λ_i, which in turn depends on the thrust coefficient.

For the normally small TPP angles encountered in helicopter flight, increasing forward speed causes the second term in Eq. (1) to increase, and its contribution to λ must be considered. In this range of small α_{TPP}, changes in inflow caused by modifications of TPP angle are proportional to μ (F. Schmitz, University of Maryland).

For TPP angles close to 90 deg arising in tiltrotor flight near airplane mode, changes in α_{TPP} have little effect on λ. This paper is not concerned with tiltrotors operating in this flight regime because BVI is not a noise source of concern near airplane mode. For inflow analysis of tiltrotors near airplane mode, see Ref. 17.

Increasing thrust can be expected to increase the mean rotor inflow. Changes in thrust arising from variations in the rotor loading will affect λ and, hence, the average miss distance. These thrust variations can be observed if, for example, part of the rotorcraft weight is shifted to existing wings, or if existing wing control surfaces are employed to generate a downforce.

Approximate Vertical Wake Displacement Model

The approximate vertical wake displacement relative to the rotor plane at a given rotor disk location is the main interest of this paper. Consider first Fig. 4. The (X, Y, Z) axes in Fig. 4 define a coordinate system that is fixed to the rotor plane. X is positive toward zero azimuth angle Ψ, Y is positive toward the advancing side, and Z is positive upward. These axes are nondimensionalized by the rotor radius R; thus, the coordinates along the (X, Y, Z) axes are expressed as a fraction of the rotor radius.

In a first level of approximation, a fluid particle initially at the disk leading edge location $(X_0, Y, 0)$ is convected along the X direction with a nondimensional speed of μ and along the Z direction with a nondimensional speed of λ. (Speeds are nondimensionalized by the blade tip speed.) In flight conditions other than sideward flight, the flow speed in the Y direction is negligible compared to the flow speed along the X and Z directions; thus the fluid particle is assumed here to travel downstream with a fixed Y. Following this simple model, the vertical displacement Z of this fluid particle as a function of X can be estimated by

$$\left(\frac{\partial Z}{\partial X}\right)_Y = \frac{-\lambda}{\mu} \tag{7}$$

Recall that the rotor inflow λ is nonuniform across the rotor disk [Eq. (3)], and it is defined as positive downward.

An approximation for the vertical displacement of the wake at a given (X, Y) point of interest in the rotor plane can be obtained by integrating Eq. (7) as X varies from X_0 to X and Z varies from 0 to Z_w; recall Y remains constant. This yields the following expression for the approximate vertical wake displacement Z_w:

$$Z_w = \underbrace{\tan(\alpha_{\text{TPP}})(X - X_0)}_{\text{inclination of the rotor}} \underbrace{- (\lambda_{i,0}/\mu)(X - X_0)\Big[\underbrace{1}_{\substack{\text{uniform}\\ \text{inflow}}} + \underbrace{k_y Y + \tfrac{1}{2}k_x(X + X_0)}_{\text{linear inflow corrections}}\Big]}_{\text{induced inflow effects}} \tag{8}$$

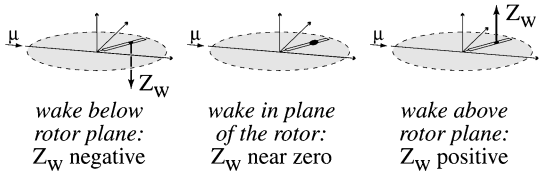

Fig. 5 Sign convention for the approximate vertical wake displacement Z_w.

where X_0 and Y remain constant and are related by the equation of a unit circle, $X_0^2 + Y^2 = 1$.

As expected, Eq. (8) shows the approximate vertical wake displacement Z_w at a given (X, Y) location in the rotor plane depends on μ, α_{TPP}, and the induced rotor inflow—hence C_T. Notice that all of the terms in Eq. (8) are nondimensional; the resulting approximate wake displacement Z_w is given as a fraction of the rotor radius R.

The first term in Eq. (8) accounts for the displacement of the fluid particle in Z due to the inclination of the rotor relative to the freestream, whereas the second term accounts for the displacement of the fluid particle in Z due to the induced inflow. This second term is further comprised of three components: The first component is the uniform induced inflow result, whereas the remaining two components arise due to the linear X- and Y-induced inflow corrections appearing in Eq. (3). These two components introduce corrections to the uniform-induced inflow result that are linear and quadratic in X. (Neglecting the variations of the induced inflow through the rotor disk normally overestimates the displacement of the fluid particle in Z, often by a factor of two.)

Equation (8) estimates the vertical wake displacement relative to the rotor disk at a chosen (X, Y) location in the rotor plane. Following the sign convention shown in Fig. 4 and as further illustrated by Fig. 5, a positive Z_w indicates the wake is above the rotor disk at the chosen (X, Y) location, whereas a negative Z_w indicates the wake is below the rotor disk at the particular (X, Y). Values for Z_w that are close to zero indicate the mean wake is near the rotor plane, and hence the miss distance is small at that (X, Y) location. The approximate wake displacement Z_w should not be considered as an exact characteristic of the wake behavior, but rather as an indicator to aid in visualizing where the mean wake is relative to the rotor plane in or near a region known to generate strong BVI.

This study presents the effects of added forces, descent angle, advance ratio, and thrust coefficient on the approximate wake displacement and thus BVI strength. The approximate vertical wake displacement Z_w at a given (X, Y) location in the rotor plane is employed as an indicator for near zero-inflow conditions, which are associated with small miss distance and hence strong BVI noise. To ease in the identification of trends, Z_w is calculated at an (X, Y) location in the rotor plane known to be representative of strong BVI generation; the figures given as examples in this paper (Figs. 9–19) are produced for (X, Y) corresponding to 65-deg azimuth angle and 85% of rotor radius.[18] If desired, the analysis methods presented in this paper could naturally be applied to other locations in the rotor disk plane.

Both helicopters and tiltrotors are considered in this analysis. Because BVI is most common in low-speed descent during a landing approach, this study focuses on advance ratios close to this operational regime. The tiltrotor analysis presented also focuses on descent approach conditions, where the nacelles are close to helicopter mode and low flight speeds limit the amount of lift the wings can carry before stall. For analysis of tiltrotor operations at higher speeds and closer to airplane mode, see Refs. 17 and 19.

For clarity when developing algebraic expressions for the approximate vertical wake displacement, this paper employs a nondimensional formulation of all variables, including the induced rotor inflow. The nondimensional induced rotor inflow λ_i depends on rotor thrust coefficient C_T, which is related to the dimensional rotor disk loading DL, air density ρ and blade tip speed by $C_T = DL/(\rho v_{\text{tip}}^2)$. Therefore, the induced rotor inflow and hence the approximate vertical wake displacement depend on rotor disk loading and air density.

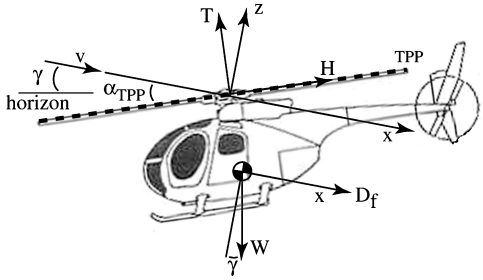

Fig. 6 Simplified helicopter free-body diagram.

In terms of its effects on λ_i and Z_w, varying C_T is equivalent to varying DL as long as ρ and v_{tip} remain unchanged. This paper presents the effects of C_T on λ_i and Z_w assuming ρ and v_{tip} are constant (most current rotorcraft operate with hover tip speeds in the vicinity of 700 ft/s, or 213 m/s). If either ρ or v_{tip} vary significantly, one would need to evaluate the dimensional induced inflow (in terms of DL and ρ) instead of the nondimensional parameters used in example Figs. 9–19 and their discussion.

For simplicity, the effects of blade flapping are neglected when studying trends in the vertical wake displacement; the rotor disk plane is considered to provide adequate information regarding the approximate location of the blades in space. However, the models to follow could be extended to account for blade flapping displacement if desired.

Trim Model

To study the effects of added forces and changes in descent angle on TPP angle, a simple trim model was developed both for helicopters and tiltrotors. The force balance equations for these rotorcraft are derived starting from a free-body diagram, and they are later solved for trim TPP angle.

Trim Model for Helicopters

A simplified free-body diagram for a helicopter is shown in Fig. 6, which was based on Ref. 9. This free-body diagram displays only the most relevant forces contributing to longitudinal and vertical force trim; other forces and moments relevant to lateral trim and moment balance are not shown. The analysis to follow makes use of only the force balance equations along the longitudinal and vertical axes; it is assumed that the pilot will adjust the rotorcraft controls to maintain pitching moment balance.

Determining the in-plane force balance equations is made a simpler task by doing so along the wind axes, where the x axis is defined along the freestream velocity vector (positive downstream) and the z axis (positive upward) is set to be perpendicular to the x axis. Note that these sets of axes becomes ill defined in hover.[9] This condition will not be treated in this paper because the present study focuses on the landing approach, the flight regime where BVI noise is most important.

Following Schmitz,[9] the free-body diagram shown in Fig. 6 yields the following trim equations.

x-force equation:

$$T \sin(-\alpha_{\text{TPP}}) - D_f - W \sin(\gamma) - H \cos(-\alpha_{\text{TPP}}) = m \frac{\mathrm{d}v}{\mathrm{d}t} \quad (9)$$

z-force equation:

$$T \cos(-\alpha_{\text{TPP}}) - W \cos(\gamma) + H \sin(-\alpha_{\text{TPP}}) = mv \frac{\mathrm{d}\gamma}{\mathrm{d}t} \quad (10)$$

To ease the interpretation and usage of the preceding expressions, it is convenient to make use of two simplifying assumptions. First, the analysis to follow is concerned with landing approaches since this is the flight regime where BVI is most important. Because of the low flight speeds associated with approach and landing, the H-force term in Eq. (9) and (10) is small compared to the other terms in the left-hand side and can be neglected. Second, the TPP angle α_{TPP} and the descent angle γ are small in typical helicopter cases and thus can be approximated as small angles.

Consequently, the trim equations (9) and (10) change as follows. Simplified x-force equation:

$$T\alpha_{\text{TPP}} + D_f + W\gamma = -m\frac{\mathrm{d}v}{\mathrm{d}t} \tag{11}$$

Simplified z-force equation:

$$T - W = mv\frac{\mathrm{d}\gamma}{\mathrm{d}t} \tag{12}$$

Solving Eq. (12) for T, substituting it into Eq. (11), and then solving for α_{TPP} yields the following expression for TPP angle[9]:

$$\alpha_{\text{TPP}} = \left(-\frac{D_f}{W} - \gamma - \frac{1}{g}\frac{\mathrm{d}v}{\mathrm{d}t}\right) \Big/ \left(1 + \frac{v}{g}\frac{\mathrm{d}\gamma}{\mathrm{d}t}\right) \tag{13}$$

Thus TPP angle is given, to a first-order approximation, by the fuselage drag as a fraction of helicopter weight, the descent angle, the acceleration along the flight path, and the flight speed times the time rate of change of the descent angle. By convention, the TPP angle is considered negative when the rotor is tilted nose down with respect to the wind speed vector (Figs. 3 and 6); thus, Eq. (13) indicates that the rotor is tilted farther down with increasing fuselage drag, climb angle, or acceleration along the flight path.

The main concern here is with steady-state approaches, where the time variations of flight speed and descent angle are small. Thus, the time-dependent terms in Eq. (13) are neglected in the analysis to follow, but they could also be considered if desired. Notice from Eq. (13) that the acceleration along the flight path normalized by gravity g has the same functional form as drag normalized by weight. Therefore, a positive acceleration along the flight path equal to a certain fraction of g has the same effect on α_{TPP} as a drag force equal to the same fraction of rotorcraft weight; the converse statement can be made regarding deceleration. For the effects of acceleration along the flight path on helicopter BVI noise, see Ref. 20.

Trim Model for Tiltrotors

A simple expression relating tiltrotor TPP angle to rotorcraft forces and descent angle is derived following steps similar to those used for a helicopter. The process starts from a simple free-body diagram, where the main forces contributing to the x- and z-force equations are considered. It is assumed that the pilot will adjust the controls to attain pitching moment balance; thus moment balance equations will not be considered when deriving an expression for TPP angle.

For simplicity, the effects of rotor downwash on the wing will not be taken into account when deriving the force equations because rotor downwash is only important for low-speed flight near helicopter mode.[10] An estimate of the minimum flight speed where the wake misses the wing can be obtained by following the trajectory of a fluid particle initially located at the centerline of the rotor disk leading edge, and calculating its approximate vertical wake displacement from Eq. (8) as it is convected downstream. Following this approach, the wake can be expected to miss the wing for advance ratios μ greater than the induced uniform inflow $\lambda_{i,0}$ for flight conditions near helicopter mode. This first-order estimate is consistent with experimental observations on a V-22 test model.[21] However, further refinements on the trim model presented in this paper could take into account the effects of rotor downwash on the wing if needed.

The wing-bound circulation generates an induced velocity field, which may affect the net rotor inflow for higher wing loadings near helicopter mode. These effects are nonuniform through the rotor disk and may slightly modify miss distance on certain BVI events in these flight contions.[17] For simplicity, the effects of wing-bound circulation on net rotor inflow are neglected in this analysis.

The resulting simplified free-body diagram for a tiltrotor is presented in Fig. 7. This free-body diagram yields the following two force balance equations, which are expressed in the rotorcraft wind axes. (The rotor thrust vector is assumed to be normal to the rotor disk plane.)

x-force equation:

$$T\sin(-\alpha_{\text{TPP}}) - D - W\sin(\gamma) - H\cos(-\alpha_{\text{TPP}}) = m\frac{\mathrm{d}v}{\mathrm{d}t} \tag{14}$$

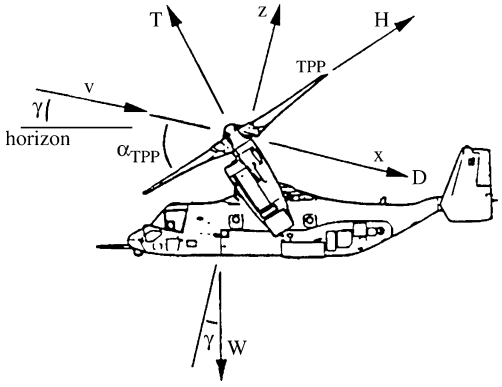

Fig. 7 Simplified tiltrotor free-body diagram.

z-force equation:

$$T\cos(-\alpha_{\text{TPP}}) - W\cos(\gamma) + L + H\sin(-\alpha_{\text{TPP}}) = mv\frac{\mathrm{d}\gamma}{\mathrm{d}t} \tag{15}$$

Equations (14) and (15) appear similar in form to the helicopter trim equations (9) and (10), with the addition of the total lift term L in the z-force equation (15). This term accounts for wing lift, tail lift, and fuselage lift. For most normal operations, fuselage and tail lift are negligible when compared to wing lift, and hence total lift is dominated by wing lift.

To simplify the algebraic manipulations to follow and thus improve the clarity of the resulting analytical model, total lift L is approximated as equal to wing lift. This simplification does not affect the general trends in the approximate vertical wake displacement Z_w that will be shown later, and it provides a model that is easier to study. If desired, the models used in this analysis could be modified to consider the separate contributions of tail, fuselage, and wing lift on total lift.

The drag term D arising in Eq. (14) represents total tiltrotor drag; it includes the drag arising from the wing, tail, fuselage and nacelles. A simplified version of this drag breakdown is used, where different drag sources are grouped into two different terms as shown in Eq. (16). The first term in this expression accounts for drag arising from wing lift, whereas the second collects all remaining drag sources that are independent of wing lift:

$$D = qSC_{D_{i,w}} + qSC_{D_{\text{other}}} \tag{16}$$

The term $C_{D_{\text{other}}}$ is a drag coefficient term that accounts for total parasite drag, tail-induced drag, and any fuselage- and nacelle-induced drag. In the present analysis, induced drag arising from the tail, fuselage, and nacelles is assumed to be small when compared to wing-induced drag and total parasite drag.

For nacelle angles below 60 deg, experimental evidence indicates nacelle drag depends on the orientation of the nacelle axis with respect to the freestream velocity vector.[22] In this case, $C_{D_{\text{other}}}$ would consist of two terms: One of them would be independent of nacelle incidence, whereas the other one would be a function of it. However, the flight conditions of interest in this study are low-speed descents during landing approach because these are the conditions where BVI is most likely to occur. Tiltrotors flying in this regime are likely to do so with nacelle angles above 60 deg, where experimental data indicate nacelle angle does not affect tiltrotor drag within experimental accuracy.[22] Drag information for the XV-15, including the influence of nacelle angle on flat plate area, can be obtained from wind-tunnel measurements.[22]

It is convenient to further simplify Eqs. (14) and (15) by means of assumptions similar to those used earlier for helicopters. Namely, the H force is assumed to be negligible, and descent angle γ can be approximated as a small angle. However, TPP angle α_{TPP} cannot be approximated as such because the tiltrotor's flexibility for tilting the nacelles allows a greater range of TPP angle values.

After making use of the these simplifying approximations, Eqs. (14) and (15) change as follows.

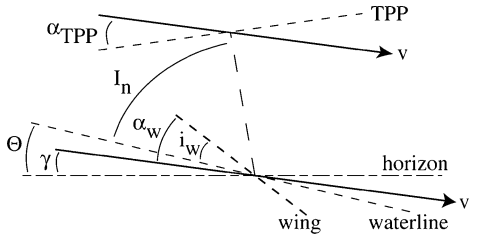

Fig. 8 Geometrical relations between angles relevant to tiltrotor analysis.

Simplified x-force equation:

$$T\sin(-\alpha_{TPP}) - D - W\gamma = m\frac{dv}{dt} \tag{17}$$

Simplified z-force equation:

$$T\cos(-\alpha_{TPP}) + L - W = mv\frac{d\gamma}{dt} \tag{18}$$

Using Eqs. (17) and (18) to eliminate T and solving for α_{TPP} results in the following expression:

$$\tan(\alpha_{TPP}) = \left(-\frac{D}{W} - \gamma - \frac{1}{g}\frac{dv}{dt}\right)\Bigg/\left(1 - \frac{L}{W} + \frac{v}{g}\frac{d\gamma}{dt}\right) \tag{19}$$

Although this formulation resembles the expression for TPP angle for helicopters— the terms in the numerator can be easily recognized to be similar to those in Eq. (13), the contribution of total lift L to the rotorcraft trim introduces a new term in the denominator. The drag term now takes into account both parasite and induced drag due to wing lift, as presented in Eq. (16). Notice also that expression (19) gives the value of the tangent of α_{TPP} instead of the angle itself; this arises from the TPP angle not being approximated as small.

The concern of this study is with steady-state approaches; hence the effects of the time-dependent terms of Eq. (19) are not considered. However, similar observations regarding the equivalence of acceleration along the flight path and added x forces can be made as in the helicopter case [Eq. (13)].

In the limiting case where α_{TPP} is small and wing lift equals zero, Eq. (19) reduces to the helicopter equation (13). Similarly, if the wing is assumed to be below stall and is carrying all of the tiltrotor weight, Eq. (19) yields a TPP angle of 90 deg. This is consistent with the tiltrotor being fully converted into airplane mode.

To relate TPP angle to nacelle angle I_n, consider the geometrical relations between some relevant tiltrotor angles shown in Fig. 8. (The wing incidence angle is measured from the fuselage waterline to the wing zero lift line,[23] and thus it is an aircraft constant.)

The following geometrical relation can be obtained from Fig. 8:

$$I_n = 90\text{ deg} - \Theta + \alpha_{TPP} + \gamma \tag{20}$$

Depending on pilot input, the tiltrotor can be trimmed with several combinations of fuselage pitch and nacelle angle for the same flight condition. The effects of choosing a specific configuration could be taken into account by including the contributions of the particular Θ and I_n on the total lift and drag terms of the trim equations.

A semi-empirical approach could be employed along with Eq. (20) to find a typical estimate for nacelle angle. The conventional variation of XV-15 fuselage pitch angle vs I_n and flight speed for a given γ can be obtained from flight-test data.[24] With use of this information, a possible value for the nacelle angle required to trim the rotorcraft for a desired α_{TPP} under a given set of flight conditions v and γ could be obtained from Eq. (20). An appropriate iteration procedure might be required.

If desired, the geometry of Fig. 8 could also be used to relate wing angle of attack to Θ, i_w, and γ, as well as to relate nacelle angle to α_{TPP}, α_w, and i_w.

Effects of Added Forces on TPP Angle and Approximate Vertical Wake Displacement for Helicopters

Starting from Eq. (13), it is of interest to find the effect that added forces have on α_{TPP} and, ultimately, on the approximate vertical wake displacement Z_w so that strategies that maximize the distance between the mean wake and the rotor plane can be identified. Added forces acting along the windstream direction (x axis in Fig. 6) will be defined as x forces, whereas added forces acting perpendicular to it (z axis in Fig. 6) will be denoted as z forces.

The general strategy to follow finds the change in TPP angle $\Delta\alpha_{TPP}$ that arises when an added force is applied to the rotorcraft. Expressions for $\Delta\alpha_{TPP}$ are derived in closed form starting from the trim equations (11) and (12), where $\Delta\alpha_{TPP}$ is defined as the final TPP angle (after applying the added force) minus the initial TPP angle (before the added force is applied). Because the sign convention for α_{TPP} defines it as negative for a nose-down tilt of the TPP (Figs. 3 and 6), a negative $\Delta\alpha_{TPP}$ corresponds to tilting the TPP in the nose-down direction, whereas a positive $\Delta\alpha_{TPP}$ corresponds to tilting the TPP in the nose-up direction.

As added forces are applied, the approximate vertical wake displacement Z_w at a chosen location in the rotor disk is estimated from Eq. (8) to identify the general trends between Z_w and added forces. Recall that Z_w is defined as positive if the wake is above the rotor plane at the location of interest and negative otherwise (Fig. 5), whereas values of Z_w close to zero indicate near-zero inflow conditions and hence high BVI likelihood.

The approximate vertical wake displacement is calculated at a location in the rotor plane known to be representative of strong BVI radiation. As already mentioned, the illustrative figures presented in this paper (Figs. 9–19) calculate Z_w at a rotor disk location corresponding to 65-deg azimuth angle and 85% of rotor radius.[18] Naturally, the approximate vertical wake displacement could be calculated at any location in the rotor disk as desired.

Added x Force (Thrust, Drag) for Helicopters

For a constant-speed approach, and assuming descent angle is maintained constant before and after applying the added force, the change in TPP angle $\Delta\alpha_{TPP}$ due to an added x force F_x is given by the following expression:

$$\Delta\alpha_{TPP} = F_x/W \tag{21}$$

Thus, the change in TPP angle equals the magnitude of the added x force expressed as a fraction of helicopter weight. An added drag force results in a negative F_x (by convention); therefore Eq. (21) shows that added drag produces a negative $\Delta\alpha_{TPP}$. This indicates that the rotor is forced to tilt farther forward to overcome the added drag and thus keep the rotorcraft in trim.

Equation (21) indicates the absolute value of $\Delta\alpha_{TPP}$ is similar for added drag and for added thrust. However, added drag and added thrust cause important different effects on the approximate vertical wake displacement Z_w and, therefore, on the average miss distance.

In the small α_{TPP} approximation and for steady flight, rotor thrust is fixed by helicopter weight as shown in Eq. (12). This indicates that an added x force does not affect T for small TPP angles, and the change in the approximate wake displacement Z_w is dominated by the first term in Eq. (8) because rotor-induced velocity effects remain roughly constant. Qualitatively, this corresponds to the wake "being roughly fixed in space," whereas the TPP is tilted forward or backward depending on the nature of the added force being employed. Therefore, it is important to consider whether the wake is initially below or above the rotor plane at the location of interest when studying the relative benefits of added drag vs added thrust.

Figure 9 shows an example of the resulting approximate wake displacement for different added x forces. As before, Z_w was calculated at a location in the rotor disk corresponding to 65-deg azimuth and 85% rotor radius. Figure 9 was generated for C_T of 0.0026 and μ of 0.13 under different descent angles. For these conditions of thrust coefficient and advance ratio and at this particular rotor location, Fig. 9 shows the mean wake is initially above the rotor plane for the steep −9-deg descent, slightly above the rotor plane for the −6-deg descent, and below the rotor plane for the shallow −3-deg descent.

If the wake is initially below the rotor (negative Z_w) at the particular location of interest in the rotor plane (for example, point A), a forward tilt of the rotor plane (due to added drag) tilts the rotor

"farther away from the wake." This causes Z_w to further increase in the negative direction; thus the miss distance at that particular location in the rotor plane increases (for example, point B). On the other hand, a backward tilt of the rotor plane (due to added thrust) tilts the rotor "into its wake." This causes Z_w to decrease; hence the miss distance at this particular location in the rotor plane decreases (for example, point C). Continuing to add thrust eventually causes the rotor to "tilt past its wake" and position itself below the wake at the location of interest; in this case Z_w becomes positive and adding more thrust causes Z_w to increase in the positive direction—hence the miss distance at the location of interest increases (for example, point E). However, if the wake is initially below the rotor plane at the location of interest, adding drag is a more attractive choice than adding thrust because the final absolute value of Z_w will be higher for the same magnitude of F_x and tilting the rotor through the wake is avoided.

If the mean wake is initially above the rotor (positive Z_w) at the location of interest in the rotor plane (for example, point G), the converse observations can be made. Adding thrust increases the miss distance at that particular location (Z_w becomes more positive) (for example, point I), whereas added drag causes the rotor plane to "tilt forward into its wake" and the miss distance decreases (for example, point J). Continuing to add drag eventually causes the rotor to "tilt forward past its wake" and Z_w becomes negative, where a farther forward tilt of the rotor disk increases the miss distance at this particular location (for example, point K). Therefore, added thrust is more attractive than added drag in cases where the wake is initially above the rotor plane at the location of interest.

Some wind-tunnel experiments to determine the drag characteristics of various added drag devices on a model helicopter fuselage are presented in Ref. 25.

Added z Force (Lift, Downforce) for Helicopters

An added vertical force F_z can be generated by a wing that may be equipped with variable control surfaces to adjust its effective angle of attack. In this case, wing stall limits dictate the maximum amount of lift or downforce that can be generated before reaching stall at the prescribed flight speed. For simplicity, it is assumed that the wing control surfaces and/or the helicopter pitch angle can be adjusted to maintain the desired F_z as α_{TPP} changes.

For a descent approach where flight speed and descent angle are kept unchanged before and after adding a z force, the change in TPP angle produced by such added lift or downforce can be found from expression (22). [Because Eq. (22) was derived starting from Eq. (13), which assumes small TPP angles, it ceases to be accurate as F_z approaches W and produces changes in TPP angle that cannot be approximated as small angles.] Thus,

$$\Delta\alpha_{\text{TPP}} = (D_f/W + \gamma)\left[1 - (1 - F_z/W)^{-1}\right] \tag{22}$$

When Eq. (22) is applied, the maximum added z force $F_{z\,\max}$ that can be generated by a wing of area S and maximum lift coefficient

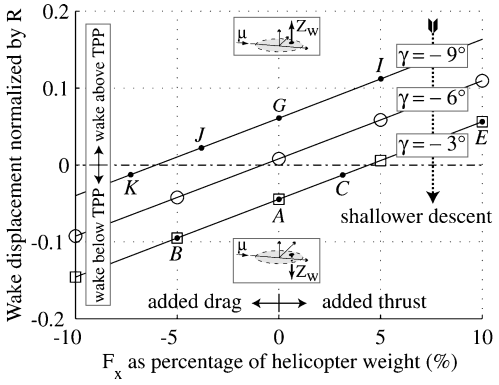

Fig. 9 Approximate vertical wake displacement vs added x force (helicopter example).

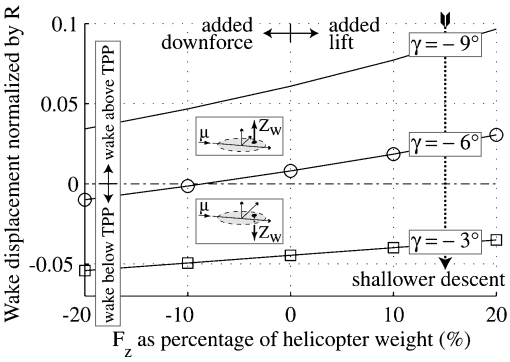

Fig. 10 Approximate vertical wake displacement vs added z force (helicopter example).

$Cl_{\max}$ before reaching stall is found from the following expression:

$$F_{z\,\max} = \pm Cl_{\max} q S \tag{23}$$

The effects of added lift on induced drag are not considered in this helicopter analysis for simplicity; thus it is assumed that the fuselage drag term in Eq. (22) is maintained constant as F_z changes. In case further refinements to this model are desired and the effects of F_z on helicopter drag are of interest, they can be found by following the procedure described in the tiltrotor section of this paper.

Unlike an added x force, an added z force will give rise to an additional term in the vertical force balance equation (12), and hence rotor thrust must be adjusted to maintain trim. This change in rotor thrust will affect the rotor-induced velocity, and thus the second term on the approximate vertical wake displacement equation (8) will be important when compared to the first. Added lift will cause a decrease in rotor thrust; hence the rotor induced velocity will decrease and the wake will not be "blown downward as strongly;" this will increase Z_w in the positive direction. On the other hand, an added downforce will cause the induced velocity to increase; hence the wake will be "blown downward more strongly," and Z_w will increase in the negative direction. Therefore, the relative benefits of added lift or downforce will depend on whether the wake is initially above or below the rotor at the location of interest in the rotor disk.

An example of the resulting approximate wake displacement Z_w for different values of added z force is presented in Fig. 10, which was generated for C_T of 0.0026 and μ of 0.13 for several descent angles. Z_w was calculated at a rotor location corresponding to 65-deg azimuth and 85% rotor radius. In Fig. 10, the added vertical force was assumed to be provided by a hypothetical wing of area equal to 5% of the rotor disk area. Maximum wing lift coefficient $Cl_{\max}$ was assumed to be 1.2; hence Eq. (23) indicates the maximum F_z that can be generated at the prescribed advance ratio is approximately equal to 20% of helicopter weight.

Cases where the mean wake is initially above the rotor at the location of interest (such as the −9-deg approach shown in Fig. 10) benefit from added lift because this decreases the rotor-induced velocity and the wake is "blown upward through the rotor" more strongly. A lower induced inflow causes the second term in Eq. (8) to be smaller; hence Z_w increases in the positive direction, and the miss distance increases at the location of interest in the rotor disk.

On the other hand, if the wake is initially below the rotor plane at the location of interest (such as the −3-deg approach shown in Fig. 10), an added downforce is more advisable because the corresponding increase in rotor induced velocity "blows the wake further downward." A higher rotor-induced inflow causes the second term in Eq. (8) to be larger, thus Z_w increases in the negative direction, and the miss distance increases at the location of interest in the rotor plane.

Added x Force Versus Added z Force for Helicopters

Figures 9 and 10 have shown that both added x and z forces can be employed to change the approximate vertical distance between the rotor and the wake at a particular location in the rotor disk known to generate strong BVI. It is now of interest to compare

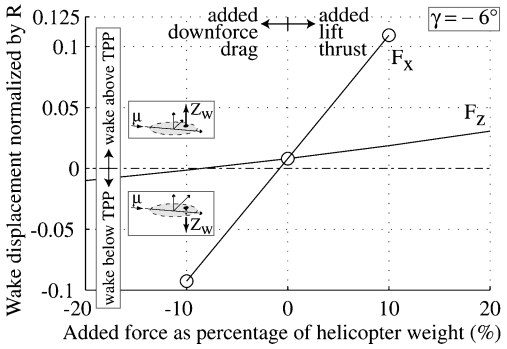

Fig. 11 Approximate vertical wake displacement vs added *x* force and *z* force (helicopter example).

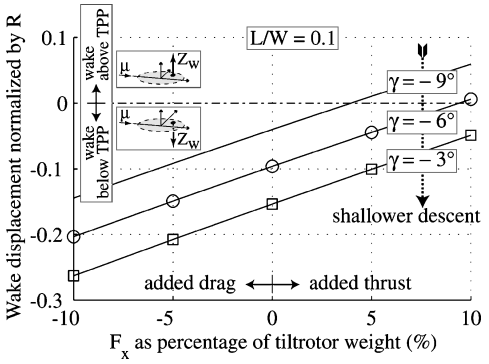

Fig. 12 Approximate vertical wake displacement vs added *x* force for varying descent angle (XV-15 example).

the relative effectiveness of these two kinds of added forces, to determine whether one of them can generate a higher absolute value of Z_w for the same magnitude of added force.

Figure 11 shows an example of the resulting approximate wake displacement for added longitudinal and vertical forces of similar magnitudes. Figure 11 was generated for a −6-deg descent, C_T of 0.0026, and μ of 0.13; Z_w was approximated at 65-deg azimuth and 85% rotor radius. These are the same flight conditions and rotor disk location that were used to produce Figs. 9 and 10. Similar stall limits for F_z as those used in Fig. 10 were employed.

As Fig. 11 indicates, added thrust (positive F_x) and added lift (positive F_z) cause Z_w to increase in the positive direction, because the rotor tilts backward and the wake is "not being blown downward as strongly," respectively. On the other hand, added drag (negative F_x) and added downforce (negative F_z) cause Z_w to increase in the negative direction, because the rotor is tilted nose down and the wake is "being blown downward more strongly," respectively. However, the Z_w vs F_x curve is much steeper than the Z_w vs F_z curve; this indicates that, for a given magnitude of added force, a higher change in Z_w can be obtained if longitudinal forces are employed. Therefore, added x forces seem a more effective mean of changing the approximate wake displacement than added z forces for the case of helicopters.

Effect of Added Forces on TPP Angle and Approximate Vertical Wake Displacement for Tiltrotors

The effects of added forces on tiltrotor TPP angle can be found starting from Eq. (19) and following essentially the same procedure used for helicopters; only the algebraic manipulation becomes more involved. This happens not only because of the extra term accounting for total lift in the trim equations, but also because TPP angle is given by a tangent function. The basic strategy is to take the arc tangent of Eq. (19) to find two expressions for α_{TPP}: one before adding forces and the other after doing so. The difference between these two expressions gives the change in TPP angle $\Delta\alpha_{\text{TPP}}$, but this result will be the difference of two inverse tangents. Thus, the final step consists on taking the tangent of both sides of the equation and making use of the appropriate trigonometric identity for the tangent of the sum of two angles.

The sign conventions introduced for added x forces (negative for drag), added z forces (positive for lift), glideslope angle (negative for descent), TPP angle (negative nose down), and approximate vertical wake displacement (positive when the wake is above the rotor disk at the rotor location of interest) remain the same as for helicopters.

Added *x* Force (Thrust, Drag) for Tiltrotors

For a constant speed, constant glideslope approach, the change in TPP angle generated by an added streamwise force is presented in Eq. (24). Notice all force terms in this expression appear as nondimensional fractions of tiltrotor weight.

Equation (24) assumes the added x force does not cause a noticeable change in total lift L. This may be achieved via fuselage-mounted drag brakes, or by using flaps or spoilers properly sized and located on both upper and lower surfaces of the wing. A modified expression will later be presented for cases where the F_x does introduce a variation in total lift. Here,

$$\tan(\Delta\alpha_{\text{TPP}}) = \frac{(F_x/W)(1 - L/W)}{(1 - L/W)^2 + (\text{D/W} + \gamma)(D/W + \gamma - F_x/W)} \tag{24}$$

For a fixed nondimensional total lift L/W, expression (24) can be shown to yield a change in TPP angle that increases in approximate linear fashion with F_x (Ref. 13) As it was the case for helicopters, added drag produces a nose-down tilt of TPP angle, whereas added thrust yields the opposite effect. Both added thrust and added drag produce similar absolute value changes in α_{TPP}, and increasing nondimensional wing lift increases the slope of the $\Delta\alpha_{\text{TPP}}$ vs F_x curves. It can also be shown that letting total lift equal to zero and approximating α_{TPP} as a small angle transforms Eq. (24) into the expression obtained for helicopters in steady flight [Eq. (21)].

For a given added x force, the change in TPP angle is higher for increasing values of wing lift.[13] Because the wing carries a more significant portion of the tiltrotor weight, less vertical component of the rotor thrust is needed to help support the rotorcraft. Thus, tiltrotors with higher wing lifts use a higher change in TPP angle to balance an added x force.

To study the trends of F_x on the approximate vertical wake displacement Z_w, consider first the case illustrated in Fig. 12. Unless otherwise noted, all tiltrotor example figures presented in this paper (Figs. 12–17) were generated for an XV-15 descending with 0.14 advance ratio. For this flight speed, wing stall limits indicate the maximum lift the wings can generate before stall [Eq. (23)] is approximately equal to 20% of tiltrotor weight. Figure 12 was generated for total lift equal to 10% of rotorcraft weight; several descent angles were included to better illustrate the effects of F_x on Z_w as γ changes. (Thrust coefficient varies slightly with F_x and γ, and it is in the range of 0.0092–0.0094 for the case in Fig. 12). All tiltrotor example figures presented in this paper (Figs. 12–17, 19) estimate the vertical wake displacement at 65-deg azimuth and 85% rotor radius; this allows for an easier comparative study between the tiltrotor and the helicopter Z_w trends.

As was the case for helicopters, added x forces do not significantly change rotor thrust, and thus the change in Z_w arising from an added longitudinal force is dominated by the first term in Eq. (8). Qualitatively, this corresponds to the wake being "approximately fixed in space," while the rotor plane tilts forward or aft depending on F_x.

Tiltrotors have a higher disk loading than helicopters. This causes a comparatively higher induced velocity, which in turn causes the wake to be below the rotor plane for a wide range of descent angles. The wake is closer to the rotor plane for steeper approaches, but rarely above the rotor plane for most conventional descents at the rotor location of interest (Fig. 12).

As Fig. 12 shows, added drag tilts the rotor farther forward and increases the separation between the rotor plane and the wake at the rotor location of interest (Z_w increases in the negative direction), whereas added thrust causes the opposite effect. This makes added drag more attractive than added thrust for most tiltrotor descent operations.

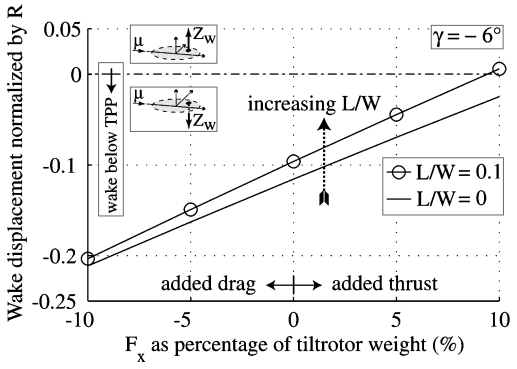

Fig. 13 Approximate vertical wake displacement vs added *x* force for varying nondimensional total lift (XV-15 example).

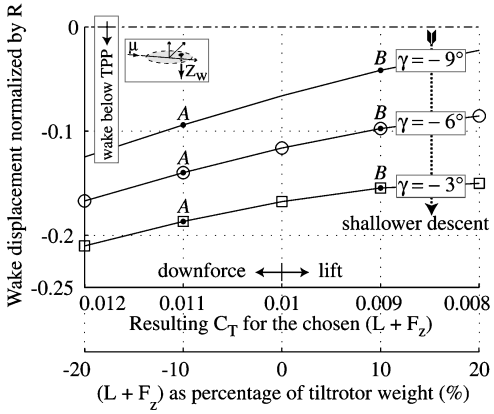

Fig. 14 Approximate vertical wake displacement vs total lift plus added *z* force for varying descent angle (XV-15 example).

The effects of F_x on Z_w for a fixed −6-deg descent angle and varying L/W are shown in Fig. 13. Figure 13 was generated for similar μ, wing stall limits, and rotor disk location as Fig. 12. (Thrust coefficient varies with F_x and L/W. For the case shown in Fig. 13, C_T is in the range of 0.0102–0.0103 for zero total lift and in the range of 0.092–0.093 for total lift equal to 10% of XV-15 weight.)

Notice from Fig. 13 that the approximate wake displacement Z_w increases in the negative direction as L/W decreases. Because the tiltrotor wing carries less lift, rotor thrust T must increase to maintain vertical force balance in steady flight [Eq. (18)]. A higher rotor thrust causes the rotor-induced velocity to increase; thus the wake is "blown downward more strongly," and Z_w increases in the negative direction [notice the second term in Eq. (8) increases due to a higher induced inflow]. Because the wake at the location of interest is initially below the rotor plane (Fig. 13), a more negative Z_w indicates the miss distance increases at this location. This suggests it is more desirable to descend with lower values of wing lift, even though Eq. (24) indicates $\Delta\alpha_{\text{TPP}}$ increases with L/W for a fixed F_x. The effects of nondimensional lift on the approximate wake displacement Z_w will be further explored in the following section.

Finally, if the added x force causes a change in lift equal to ΔL, the following expression can be used instead of Eq. (24) to account for this effect:

$$\tan(\Delta\alpha_{\text{TPP}}) = \frac{(F_x/W)(1 - L/W) - (\Delta L/W)(D/W + \gamma)}{(1 - L/W)(1 - L/W - \Delta L/W) + (D/W + \gamma)(D/W + \gamma - F_x/W)} \tag{25}$$

Added *z* Force (Lift, Downforce) for Tiltrotors

The change in tiltrotor TPP angle produced by an added z force can be found following a procedure similar to that presented for added x forces. Because induced drag is dependent on lift squared, changes in drag must be taken into account when introducing added z forces.

For a constant speed, constant glideslope descent, the change in TPP angle resulting from an added z force at a given initial value of total nondimensional lift is given by

$$\tan(\Delta\alpha_{\text{TPP}}) = \frac{-(F_z/W)(D/W + \gamma) - (\Delta D/W)(1 - L/W)}{(1 - L/W)(1 - L/W - F_z/W) + (D/W + \gamma)(D/W + \gamma + \Delta D/W)} \tag{26}$$

The terms L/W appearing in Eqs. (26) and (27) and the term D/W in Eq. (26) represent total nondimensional lift and drag, respectively, before adding F_z. The term ΔD in Eq. (26) accounts for the change in drag introduced by F_z, so that total rotorcraft drag equals D before adding the vertical force and $(D + \Delta D)$ after doing so. Initial tiltrotor drag D is found from Eq. (16), whereas the change in drag ΔD is given by the following expression:

$$\frac{\Delta D}{W} = \frac{W}{qS\pi ARe}\left(\frac{F_z}{W}\right)\left(2\frac{L}{W} + \frac{F_z}{W}\right) \tag{27}$$

where e is the wing Oswald efficiency factor. Experimental measurements for the XV-15 have found that e varies with nacelle angle: It equals 0.987 for airplane mode[24] and 0.893 for helicopter mode (M. Maisel, NASA Ames Research Center). For the example figures presented in this paper (Figs. 12–17), e is taken as the helicopter mode value of 0.893.

To study the trends of F_z on the approximate vertical wake displacement Z_w, consider the case shown in Fig. 14. Figure 14 was generated for an XV-15 descending with 0.14 advance ratio. At this flight speed, recall stall considerations limit wing lift to be below approximately 20% of tiltrotor weight. Z_w was calculated at a rotor location corresponding to 65-deg azimuth and 85% rotor radius.

As has been discussed, the tiltrotor wake is initially below the rotor plane for most conventional descent approach angles at the rotor location of interest (Figs. 12–14) due to the high rotor-induced velocity. A vertical force that does not violate stall limits causes a relatively small change in α_{TPP} (Ref. 13), but it effectively modifies the total nondimensional lift term of the vertical force balance equation (18). As a consequence, rotor thrust must be adjusted (as also shown in Fig. 14) and the rotor-induced velocity changes. This introduces an effect in Z_w through the second term of Eq. (8).

An added downforce effectively translates into reducing wing lift or even causing it to become negative (within wing stall bounds). This generates an increase in rotor-induced velocity because more rotor thrust is needed to overcome the effective increase in tiltrotor weight. The increase in rotor-induced velocity causes the mean wake to be "blown downward more strongly," hence Z_w increases in the negative direction, and the miss distance increases at the rotor location of interest (Fig. 14). Adding lift causes the opposite effect; thus a negative F_z (that is, reducing wing lift or causing it to become negative) seems a more attractive alternative than a positive F_z (that is, increasing wing lift) for most tiltrotor descent operations. This is shown in Fig. 14, which also suggests shallower approaches are more desirable if the average miss distance is to be maximized at this particular rotor location.

The initial lift before adding a z force determines the point along the curve in Fig. 14 where the tiltrotor initially operates. Thus, for example, a configuration that has an initially low L can afford a higher added lift (positive F_z) before approaching $Cl_{\max}$ (for example, point A), whereas a configuration with initially higher L can accept a

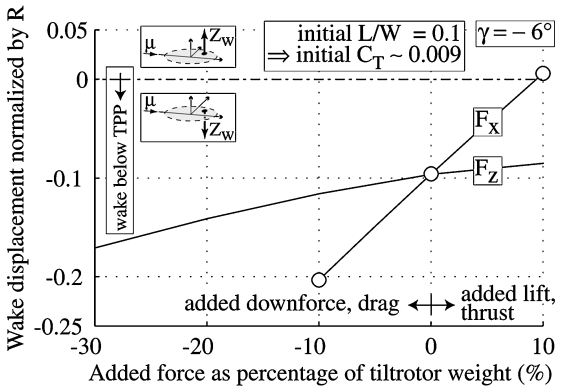

Fig. 15 Approximate vertical wake displacement vs added *x* force and *z* force (XV-15 example).

higher downforce (negative F_z) before nearing stall (for example, point B).

Added *x* Force Versus Added *z* Force for Tiltrotors

Both added drag and added downforce have been shown to cause a favorable increase in $|Z_w|$ at the rotor location of interest; it seems natural now to compare these two techniques to identify which one is more effective. Figure 15 is a comparison of the effects of F_x and F_z on Z_w for an XV-15 descending along a −6-deg glideslope with initial total lift equal to 10% of tiltrotor weight and initial C_T of 0.009. Advance ratio, wing stall limits and rotor disk location are similar to those employed to generate Figs. 12–14.

As a vertical force is added, $(L + F_z)$ changes, and rotor thrust must be properly adjusted to maintain vertical force balance. This causes C_T to vary from its initial value of 0.009 as F_z moves away from zero in Fig. 15: C_T increases to 0.012 when the added downforce reaches 30% of tiltrotor weight and decreases to 0.008 when the added lift equals to 10% of tiltrotor weight. On the other hand, an added x force does not significantly change rotor thrust for a fixed L; hence, C_T remains within 2% of its initial value along the added x force line.

For a given magnitude of added force, Fig. 15 suggests added x forces can generate a higher change in Z_w than added z forces. (This observation is similar to the one made for the helicopter case.) Therefore, Fig. 15 indicates added drag is more attractive than added downforces. Note, however, that both techniques are not necessarily mutually exclusive and could possibly be employed simultaneously for added benefits (for example, a tiltrotor could deploy its drag brakes while adjusting its wing surfaces and elevators to minimize wing lift or even generate a downforce).

Effects of Changing Descent Angle on TPP Angle and Approximate Vertical Wake Displacement

The trim expressions (13) (helicopters) and (19) (tiltrotors) and the approximate vertical wake displacement equation (8) show α_{TPP} and Z_w depend on descent angle γ; Figs. 9 and 10 (helicopter example), as well as Figs. 12 and 14 (XV-15 example) further illustrate the dependence of Z_w on γ. In cases where regulations do not constrain glideslope descent angle, choosing to land with a different γ might be a more practical alternative than installing added force devices on a helicopter. Tiltrotors can also benefit from properly adjusting γ, particularly in cases where added forces can also be used for further benefit. Therefore, is of interest to consider the effects of γ on α_{TPP} and, ultimately, on Z_w with more care.

The general steps employed to derive a closed-form equation that relates $\Delta\alpha_{\text{TPP}}$ to a change in descent angle $\Delta\gamma$ are similar to those used in the preceding sections to find expressions for $\Delta\alpha_{\text{TPP}}$ as a function of added forces. By convention, γ is negative for descent; hence, a negative $\Delta\gamma$ corresponds to a steeper approach, whereas a positive $\Delta\gamma$ implies a shallower descent.

To better study the effects of descent angle on TPP angle and the approximate vertical wake displacement, flight speed is maintained constant as γ is varied; the effects of changing μ are considered later in this paper.

Vertical rate of sink (ROS) is related to forward flight speed v and descent angle γ by the following expression:

$$\text{ROS} = v\sin(-\gamma) \underset{(\text{for small }\gamma)}{\approx} -v\gamma \tag{28}$$

For a constant flight speed, Eq. (28) shows that landing with a steeper approach increases the vertical rate of sink. This may be acceptable as long as ROS does not increase past some acceptable maximum value for safety, thus introducing a constraint on the steepest descent that can be flown for a given flight speed. As an illustration, a maximum ROS of 1000 ft/min (5.08 m/s) is assumed, as suggested by W. Decker (NASA Ames Research Center).

For a helicopter descending at constant flight speed and if the proposed $\Delta\gamma$ does not violate the maximum ROS constraint, the change in TPP angle introduced by a change in descent angle is given by Eq. (29). This expression was derived starting from Eq. (13), which assumes small angles. Recall a negative $\Delta\alpha_{\text{TPP}}$ corresponds to a change in α_{TPP} in the nose-down direction, whereas a positive $\Delta\alpha_{\text{TPP}}$ corresponds to a change in the nose-up direction.

Helicopter:

$$\Delta\alpha_{\text{TPP}} = -\Delta\gamma \tag{29}$$

Equation (29) indicates a shallower descent (positive $\Delta\gamma$) corresponds to a relative nose down tilt of the rotor plane (negative $\Delta\alpha_{\text{TPP}}$), whereas a steeper descent (negative $\Delta\gamma$) corresponds to a relative nose up tilt of the rotor plane (positive $\Delta\alpha_{\text{TPP}}$). Notice from Eq. (29) that, whether the change in descent angle is positive or negative, the resulting change in TPP angle is equal in magnitude to $\Delta\gamma$ when flight speed remains unchanged. Comparing Eqs. (21) and (29) shows the equivalence of added longitudinal forces and changes in descent angle as means of varying helicopter TPP angle.[13]

From a physical standpoint, changing descent angle corresponds to varying the incidence of the freestream velocity vector (Fig. 6), while the TPP remains "fixed in space." This introduces important effects on the approximate vertical wake displacement Z_w, which will be affected by the first term of Eq. (8).

For a tiltrotor descending at constant flight speed and if the proposed $\Delta\gamma$ does not violate the maximum ROS constraint, the change in TPP angle generated by a change in descent angle is given by Eq. (30).

Tiltrotor:

$$\tan(\Delta\alpha_{\text{TPP}}) = \frac{-\Delta\gamma(1 - L/W)}{(1 - L/W)^2 + (D/W + \gamma)(D/W + \gamma + \Delta\gamma)} \tag{30}$$

The term γ in Eq. (30) represents the initial descent angle, so that $(\gamma + \Delta\gamma)$ equals the final descent angle. Varying γ changes the

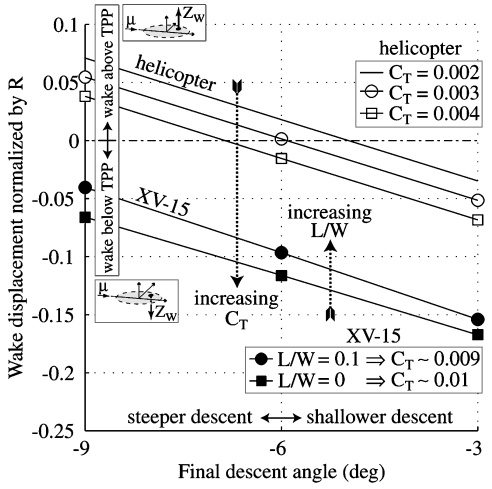

Fig. 16 Approximate vertical wake displacement vs descent angle for several thrust coefficients (helicopter and XV-15 example).

relative incidence of the freestream velocity vector with respect to the rotorcraft (Fig. 7); hence total lift L and drag D could change with γ depending on the choice of trim. However, to better illustrate the effects of descent angle on α_{TPP} and thus Z_w, Eq. (30) assumes the appropriate control surfaces are adjusted so that L remains constant, and the change in drag caused by $\Delta\gamma$ is small and can be neglected.

The effects of varying descent angle on the approximate vertical wake displacement are shown in Fig. 16 for both a helicopter and a tiltrotor example. Figure 16 was generated for an advance ratio of 0.14; the 1000-ft/min (5.08 m/s) maximum ROS constraint is not violated at this flight speed for all descent angles shown in Fig. 16. The vertical wake displacement was estimated at a rotor location corresponding to 65-deg azimuth and 85% rotor radius.

The tiltrotor curves in Fig. 16 correspond to different values of total lift, and hence to different values of rotor thrust coefficient as dictated by vertical force balance [Eq. (18)]. To aid in visualizing the dependence of Z_w on γ, Fig. 16 assumes total tiltrotor lift remains constant as γ varies. Tiltrotor wing stall limits are similar to those employed to generate Figs. 12–15; several helicopter thrust coefficients are also shown. (As γ changes, tiltrotor C_T stays within 1% of the average values shown in Fig. 16.)

The vectorial component of flight speed normal to the rotor plane $v\sin(\alpha_{\text{TPP}})$ points upward if α_{TPP} is positive and downward if α_{TPP} is negative. If TPP angle is positive, a steeper descent causes a stronger upward $v\sin(\alpha_{\text{TPP}})$; if TPP angle is negative, a steeper descent translates into a lower downward $v\sin(\alpha_{\text{TPP}})$. Both cases will cause the mean wake to move upward relative to the rotor plane, which causes Z_w to increase in the positive direction.

For helicopters, choosing a steeper or shallower approach to maximize Z_w depends on the initial location of the wake relative to the rotor at the location of interest in the rotor disk. Lower values of C_T are likely to start with the wake slightly above the rotor plane at the location of interest; in this case steeper approaches "further blow the wake above the rotor" and hence increase Z_w in the positive direction. On the other hand, higher values of C_T are more likely to cause the wake to be below the rotor at the location of interest; in this case a shallower approach seems more attractive. For all descent angles, increasing thrust coefficient causes a stronger downward induced velocity, hence shifting the Z_w curves in Fig. 16 to a more negative value. This suggests shallow approaches are specially desirable for higher thrust coefficients.

The higher rotor-induced velocity associated with tiltrotor C_T near helicopter mode causes the tiltrotor wake to be "blown downward more strongly" than for helicopters; thus the approximate vertical wake displacement is more negative for tiltrotors than for helicopters under all descent angles shown in Fig. 16. Unlike helicopters, the tiltrotor mean wake is normally below the rotor plane for normal descent operations near helicopter mode; this makes shallower descents more desirable than steeper descents for the tiltrotor cases shown in Fig. 16.

Effects of Advance Ratio and Thrust Coefficient on Approximate Vertical Wake Displacement

To better identify the general trends of Z_w with varying rotorcraft forces or changes in descent angle, the analysis presented in the preceding sections has been performed for a fixed flight speed, hence a fixed advance ratio. However, the approximate vertical wake displacement is a function of advance ratio μ as illustrated by Eq. (8). Properly adjusting the approach speed may be a practical tool to increase $|Z_w|$ and hence the average miss distance; thus it is of interest to consider this with more care.

Figure 17 presents contours of the approximate vertical wake displacement Z_w vs advance ratio μ and thrust coefficient C_T for both a helicopter and a tiltrotor example descending along various glideslope angles. To better focus on flight conditions corresponding to lower speed descents, Fig. 17 only shows Z_w for ranges in μ that correspond to flight speeds approximately between 40 and 70 kn. The vertical wake displacement shown in Fig. 17 was estimated for a rotor location corresponding to 65-deg azimuth and 85% rotor radius.

The helicopter Z_w contours were found by choosing (μ, C_T) pairs, solving for TPP angle from Eq. (13), and using these parameters to find Z_w from Eq. (8). The tiltrotor Z_w contours were obtained by choosing (μ, C_T) pairs, employing an iterative procedure with the force balance equations (17) and (18) [as well as the drag equation (16)] to find trim TPP angle, total lift and drag, and finally using Eq. (8) to find Z_w.

For a given μ, the low C_T boundary for the tiltrotor case in Fig. 17 is given by wing stall. Maximum wing lift coefficient was assumed equal to 1.2 in Fig. 17; this stall limitation is similar to that employed when generating Figs. 12–16. The maximum advance ratio boundary appearing in the −9-deg descent case of Fig. 17 arises from a 1000-ft/min (5.08 m/s) maximum rate of sink constraint; this was implemented following Eq. (28).

The higher values of thrust coefficient characteristic of tiltrotors place their Z_w curves along the upper range of the C_T axis in Fig. 17, whereas the lower thrust coefficients corresponding to helicopter flight appear on the lower range of the C_T axis. The shaded region in Fig. 17 indicates conditions where the wake is above the rotor at the location of interest in the rotor plane; notice these occur for certain helicopter cases while the tiltrotor wake is below the rotor for all conditions illustrated in Fig. 17.

Figure 17 suggests that descending with lower μ, higher C_T, and shallower γ normally increase $|Z_w|$ in cases where the mean wake is initially below the rotor plane. On the other hand, lower C_T and steeper γ increase $|Z_w|$ in cases where the mean wake is initially above the rotor plane. In these cases where Z_w is initially positive, μ has no significant effect on $|Z_w|$ except for steep descents, where higher μ can increase $|Z_w|$ (Fig. 17).

In the helicopter case shown in Fig. 17, the vertical wake displacement is sensitive to both advance ratio and thrust coefficient

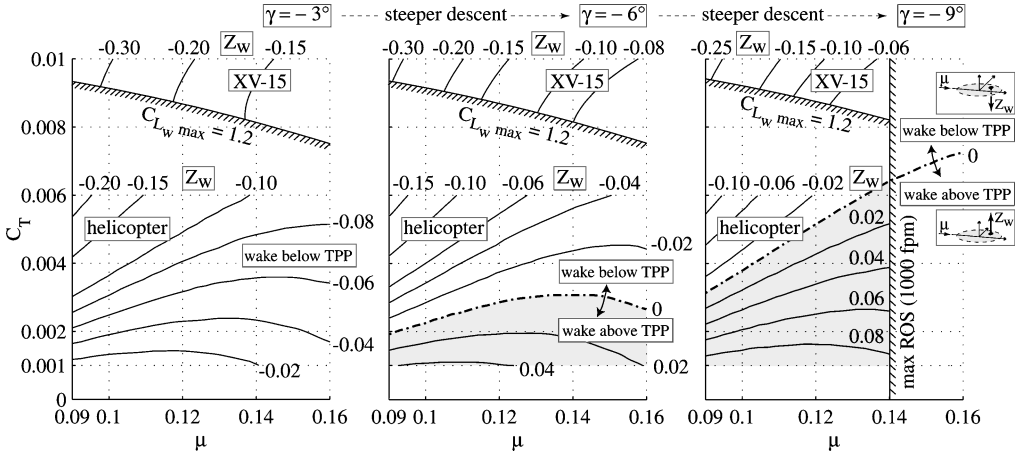

Fig. 17 Contour plot of the approximate vertical wake displacement vs advance ratio and thrust coefficient for different descent angles (helicopter and XV-15 example).

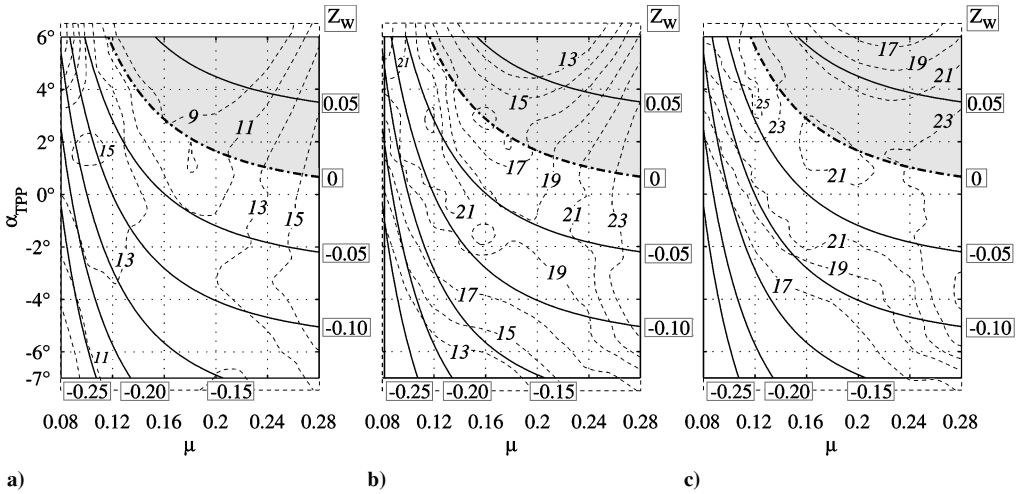

Fig. 18 Approximate vertical wake displacement contours superimposed on experimental BVISPL contour plots (decibels minus 80 dB) from Ref. 26, with experimental data taken a) upstream the retreating side, b) upstream center, and c) upstream the advancing side (helicopter example).

for low flight speeds. As μ increases, changes in flight speed have a smaller effect on Z_w than changes in thrust coefficient. Note from Eq. (12) that helicopter thrust (hence C_T) is normally fixed by weight in steady-state flight; this suggests one can more easily "move between" the helicopter Z_w contours of Fig. 17 by adjusting advance ratio or descent angle while C_T remains constant.

On the other hand, tiltrotors may afford a change in rotor thrust because total lift L may be adjusted to balance the rotorcraft in steady-state z-force trim [Eq. (18)]. However, Fig. 17 suggests the tiltrotor approximate vertical wake displacement is more sensitive to changes in μ for all flight speeds, whereas changes in C_T produce a comparatively lower effect in Z_w.

As the descent angle γ becomes steeper, the upward component of the freestream velocity vector increases, and the wake is "blown upwards more strongly." As a consequence, the portion of the (μ, C_T) flight envelope where the wake is above the rotor at the location of interest increases. This region is shaded in Fig. 17; notice that it becomes important for helicopter flight at steep descent angles. Figure 17 also shows the region in the (μ, C_T) space where the wake is near the rotor at the location of interest is smaller for the shallow -3-deg descent case; this suggests near-zero inflow conditions at this particular rotor location are less likely if γ is shallow.

Notice that the general shape of the approximate wake displacement contours is generally similar as γ varies, but the Z_w values of these contours change with γ. In this regard, varying descent angle could be thought of approximately as a shift in the Z_w vs (μ, C_T) contours.

Experimental Illustration

Possible alternatives have been presented for maximizing the separation between the wake and the rotor at a particular location in the rotor plane known to generate BVI. These strategies have been evaluated considering that, other parameters being equal, BVI strength at a particular rotor location decreases with increasing $|Z_w|$ because the vertical separation between the wake and the rotor is higher. To verify this assumption and evaluate the usefulness of Z_w as a general indicator of BVI likelihood at a particular rotor location, it is of interest to compare trends in Z_w vs existing experimental noise data.

Before proceeding, a general caveat must be made. The experimental BVI data to be presented capture the total rotor noise signature, which includes BVI noise from several interactions at different locations in the rotor disk as well as other noise sources. These data will be compared with values of Z_w that were calculated at a single rotor location (65-deg azimuth and 85% rotor radius); this region in the rotor disk can be considered representative of BVI generation,[18] but the values of Z_w obtained here may not correspond exactly to other rotor locations where BVI occur. However, choosing a single rotor location to calculate Z_w allows for an easier evaluation of its general usefulness.

Also note that the vertical wake displacement is an analytical tool that is simple to implement and study; it was developed to aid in the identification and understanding of trends. Naturally, it does not capture all of the details of the full BVI problem.

Experimental Illustration for Helicopters

BVI sound pressure level (BVISPL) contours vs μ and C_T have been obtained by Burley and Martin.[26] These experiments were made for a four-bladed, 40% scale model of a BO-105 rotor operating at 0.0044 C_T in a wind tunnel. Noise was obtained at different observer locations at a distance from the hub equal to 1.25 rotor radii.

To illustrate the usefulness of Z_w as an indicator of BVI likelihood, contours of Z_w were calculated for each $(\mu, \alpha_{\text{TPP}})$ pair using Eq. (8) and superimposed into the experimental contour plot. This is shown in Fig. 18.

BVISPL contours vs $(\mu, \alpha_{\text{TPP}})$ are shown in dashed lines in Fig. 18; their magnitude minus 80 dB is shown in the corresponding inline labels. Approximate vertical wake displacement contours are superimposed as solid lines, and their value is shown inside text boxes next to the contours. The values for Z_w shown represent the approximate wake displacement normalized by rotor radius; they were calculated at a rotor location corresponding to 65-deg azimuth and 85% rotor radius. The shaded area in Fig. 18 represents the region in $(\mu, \alpha_{\text{TPP}})$ space where the wake is above the rotor at this particular location in the rotor disk.

The simple Z_w contours at a single rotor location naturally cannot capture all of the complexities of the experimental BVI noise contours. However, BVI levels tend to decrease in the general direction of increasing $|Z_w|$, and they tend to increase in the general direction where Z_w approaches zero. (Notice the agreement between the Z_w contours and the experimental noise contours is better for the lower advance ratios, which correspond to lower advancing tip Mach numbers.) As already mentioned, a higher value of $|Z_w|$ indicates the vertical distance between the wake and the rotor is higher at the location of interest, whereas values of Z_w close to zero correspond to near-zero inflow conditions where the wake is close to the rotor plane.

For the three measurement locations shown in Fig. 18, notice the agreement between experimental data and Z_w trends is better for Fig. 18c, where the BVI noise levels are higher. This corresponds to a microphone located upstream of the advancing side. Directionality studies have shown this is the general location where strong BVI radiates.[5,27]

Experimental Illustration for Tiltrotors

Wind-tunnel noise data for an isolated, full-scale XV-15 rotor near helicopter mode are presented by Kitaplioglu.[28] Some of these data are plotted in Fig. 19, which shows BVISPL contours vs

Table 1 Qualitative effects of added forces, descent angle, thrust coefficient, and advance ratio on TPP angle, induced inflow, and approximate vertical wake displacement

Technique for modifying Z_w	Effect on α_{TPP} (direction of tilt)	Effect on λ_i (induced inflow)	Effect on Z_w (direction of change)	Useful for wake initially above or below rotor	Notes
Added forces					
F_x drag	Nose down	Little effect	Downward (−ve)	Below	
F_x thrust	Nose up	Little effect	Upward (+ve)	Above	
F_z lift	Little effect	Decreases	Upward (+ve)	Above	Less effective than thrust
F_z downforce	Little effect	Increases	Downward (−ve)	Below	Less effective than drag
Changes in γ					Constrained by max.
Steeper descent	Nose up	Little effect	Upward (+ve)	Above	ROS. Easier to implement
Shallower descent	Nose down	Little effect	Downward (−ve)	Below	than added forces for helicopters
Changes in C_T					
Increase	Little effect	Increases	Downward (−ve)	Below	C_T fixed for helicopters in
Decrease	Little effect	Decreases	Upward (+ve)	Above	steady flight
Changes in μ					
Slower approach	Nose up	Increases	Downward (−ve)	Below	Effect on Z_w
Faster approach	Nose down	Decreases	Varies	Varies	depends of γ (Fig. 17)

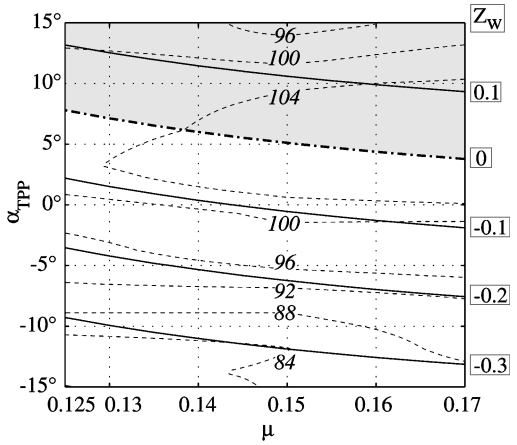

Fig. 19 Approximate vertical wake displacement contours superimposed on experimental BVISPL contour plots generated from data in Ref. 28 (XV-15 example).

(μ, α_{TPP}) upstream the advancing side at a ground location 6 rotor radii away from the rotor hub. Thrust coefficient for the data shown in Fig. 19 is approximately 0.0067.

The dashed lines in Fig. 19 represent noise levels from experimental data[28]; their magnitude (in decibels) is shown in the respective inline labels. The solid lines are contours of the approximate vertical wake displacement Z_w; these were calculated using Eq. (8) for each (μ, α_{TPP}) pair and then superimposed onto the experimental contours for illustration. Z_w values are shown in the legend boxes next to the corresponding contour lines; these were calculated at a location in the rotor disk corresponding to 65-deg azimuth and 85% rotor radius.

Note that neither the experimental results nor the calculated Z_w values in Fig. 19 capture the effects of rotor downwash on the wing. However, rotor downwash is not an important effect at the advance ratios shown in Fig. 19. For an XV-15 in helicopter mode under the flight conditions corresponding to Fig. 19, the rotor wake is "blown behind the wing" for advance ratios greater than approximately 0.06; notice this is roughly half the minimum μ shown in Fig. 19.

As Fig. 19 shows, BVI levels tend to decrease in the general direction of increasing $|Z_w|$, and they tend to increase in the general direction where Z_w approaches zero. This is a similar observation to that made in the helicopter illustration of Fig. 18.

Synopsis

The qualitative effects of added forces, descent angle, advance ratio and thrust coefficient are summarized in Table 1. For conventional descents near the helicopter configuration, recall that the tiltrotor wake is likely below the rotor plane at the location of interest (Fig. 17). Therefore, the techniques labeled as useful when the wake is below the rotor plane are particularly appropriate for tiltrotors.

Conclusions

Trends concerning the vertical separation between the wake and the rotor at any particular location of interest in the rotor plane can be identified with the aid of the approximate vertical wake displacement. This simple analytical technique can be employed to understand the potential effects of added forces, descent angle, thrust coefficient, and advance ratio on the relative separation between the wake and the rotor at any point in the rotor plane known to be significant for BVI noise.

The vertical location of the wake relative to the rotor plane is a strong function of the rotor-induced velocity. Tiltrotors in conventional descent approaches near helicopter mode have a high disk loading; the resulting induced velocity field is strong, and the wake is likely to be below the rotor plane. In contrast, helicopters have a comparatively lower disk loading and their induced velocity field is not as strong; hence their wake may be above or below the rotor disk depending on flight conditions (advance ratio, descent angle) and helicopter parameters (thrust coefficient) for a steady approach.

The relative benefits of added forces, choice of descent angle, advance ratio, and thrust coefficient depend on whether the rotorcraft wake is initially above or below the rotor plane at the rotor location of interest. Cases where the wake is below the rotor plane benefit from added drag, added downforces, shallower approaches, lower advance ratios, and higher thrust coefficients. Tiltrotors during descent operations benefit from these techniques, as well as helicopter descent approaches under higher thrust coefficients, lower advance ratios, and/or shallower descent angles.

On the other hand, cases where the wake is initially above the rotor plane are likely to benefit from added thrust, added lift, steeper approaches, higher advance ratios, and lower thrust coefficients. These cases may arise in certain helicopter descent approaches under lower thrust coefficient, higher advance ratio, and/or steeper descent conditions.

For both helicopters and tiltrotors, added longitudinal forces are preferable over added vertical forces of the same magnitude because they have a more significant effect on the vertical separation between the wake and the rotor. Tiltrotors benefit from lower values of total lift, since the consequent increase in rotor thrust further increases the separation between the wake and the rotor.

The different techniques presented to maximize the distance between the wake and the rotor are not mutually exclusive, and they could be employed simultaneously for maximum combined effect. For example, a tiltrotor could increase drag, reduce wing lift (or even make it negative if possible), reduce flight speed, and land with a shallower descent angle.

A linear inflow model has been employed when deriving an expression for the approximate vertical wake displacement. If desired, a different inflow model—analytical computational, or empirical—could be used.

For simplicity and clarity, example Figs. 9–19 were presented for the approximate vertical wake displacement at a representative location in the rotor disk. However, the approximate vertical wake displacement could be calculated at several rotor locations known to generate BVI, so that strategies that maximize it in all of these could be identified.

Finally, the effects of thrust coefficient on the approximate vertical wake displacement have been discussed assuming that air density and blade tip speed remain unchanged. If either of these two parameters varies, the induced inflow effects should be evaluated using dimensional variables.

Acknowledgments

This research work has been supported by the U.S. Army Research Office under Multi-University Research Initiative (MURI) Grant DAAH-04-96-10334 with Gary Anderson as Technical Monitor. The authors would like to specially thank Fredric Schmitz (University of Maryland) for his comments at various stages of this research; his valuable insights greatly contributed to improve the relevance of this work. The authors would also like to thank Ben W.-C. Sim (University of Maryland), as well as William Decker, Cahit Kitaplioglu, and Martin Maisel (NASA Ames Research Center) for their valuable and timely information and input.

References

[1]George, A. R., "Helicopter Noise: State-of-the-Art," *Journal of Aircraft*, Vol. 15, No. 11, 1978, pp. 707–715.

[2]Schmitz, F. H., "Rotor Noise," *Aeroacoustics of Flight Vehicles: Theory and Practice*, Vol. 1, NASA RP-1258, 1991, Chap. 2.

[3]Baeder, J., and Sim, B. W.-C., "Blade–Vortex Interaction Noise Reduction by Active Trailing Edge Flaps," American Helicopter Society 54th Annual Forum and Technology Display, Washington, DC, May, 1998.

[4]Tangler, J. L., "Schlieren and Noise Studies of Rotors in Forward Flight," American Helicopter Society 33rd Annual Forum and Technology Display, Paper 77.33-5, Washington, DC, May 1977.

[5]Ringler, T. D., George, A. R., and Steele, J. B., "A Study of Blade–Vortex Interaction Sound Generation and Directionality," American Helicopter Society's International Technical Specialists Meeting, Valley Forge, Pennsylvania, Oct. 1991.

[6]Sim, B. W.-C., and George, A. R., "Development of a Rotor Aerodynamic Load Prediction Scheme for Blade–Vortex Interaction Noise Study," *Proceedings of the American Helicopter Society 51st Annual Forum and Technology Display*, AHS International, Alexandria, VA, 1995, pp. 525–546.

[7]Sim, B. W.-C., George, A. R., and Yen, S. J., "Blade–Vortex Interaction Noise Directivity Studies Using Trace Mach Number," American Helicopter Society 2nd Aeromechanics Specialists Meeting, Oct. 1995.

[8]Sim, B. W.-C., and George, A. R., "Investigation of Caustics Propagation in Blade–Vortex Interaction Noise," American Helicopter Society 53rd Annual Forum and Technology Display, April–May, 1997.

[9]Schmitz, F. H., "Reduction of Blade–Vortex Interaction (BVI) Noise Through X-Force Control," *Journal of the American Helicopter Society*, Vol. 43, No. 1, 1998, pp. 14–24.

[10]George, A. R., Smith, C. A., Maisel, M. D., and Brieger, J. T., "Tilt Rotor Aircraft Aeroacoustics," American Helicopter Society 45th Annual Forum and Technology Display, Boston, Massachusetts, May 1989.

[11]Jacobs, E. W., Chen, R. T. N., and Santa María, O. L., "The Development and Flight Test Demonstration of Noise Abatement Approach Procedures for the Sikorsky S-76," American Helicopter Society Technical Specialists Meeting for Rotorcraft Acoustics and Aerodynamics, Oct. 1997.

[12]JanakiRam, R. D., O'Connel, J. M., Fredrickson, D. E., Conner, D. A., and Rutledge, C. K., "Development and Demonstration of Noise Abatement Approach Flight Operations for a Light Twin-engine Helicopter—MD Explorer," American Helicopter Society Technical Specialists Meeting for Rotorcraft Acoustics and Aerodynamics, Oct. 1997.

[13]Abelló, J. C., and George, A. R., "Rotorcraft BVI Noise Reduction by Attitude Modification," AIAA Paper 99-1931, May 1999.

[14]Abelló, J. C., and George, A. R., "Wake Displacement Study of Attitude and Flight Parameter Modifications to Reduce Rotorcraft Blade-Vortex Interaction (BVI) Noise," *9th AIAA/CEAS Aeroacoustics Conference*, AIAA 2003-3174, Hilton Head, South Carolina, May 2003.

[15]Leishman, J. G., *Principles of Helicopter Aerodynamics*, Cambridge Univ. Press, Cambridge, England, U.K., 2000, pp. 116–123.

[16]Drees, J. M., "A Theory of Airflow Through Rotors and Its Application to Some Helicopter Problems," *Journal of the Helicopter Association of Great Britain*, Vol. 3, No. 2, 1949, pp. 79–104.

[17]Gervais, M., "Tiltrotor Blade–Vortex Interaction (BVI) Noise Control Through Non-Unique Longitudinal Force Trim," Southeast Lichten Award Regional Competition of the American Helicopter Society, Jan. 2001.

[18]Splettstoesser, W. R., Schultz, K. J., and Martin, R. M., "Rotor Blade-Vortex Interaction Impulsive Noise Source Localization," *AIAA Journal*, Vol. 28, No. 4, 1990, pp. 593–600.

[19]Gervais, M., and Schmitz, F. H., "Tiltrotor BVI Noise Reduction Through Flight Trajectory Management and Configuration Control," AIAA Paper 2002-2544, June 2002.

[20]Schmitz, F. H., Gopalan, G., and Sim, B. W.-C., "Flight-Path Management/Control Methodology to Reduce Helicopter Blade–Vortex Interaction Noise," *Journal of Aircraft*, Vol. 39, No. 2, 2002, pp. 193–205.

[21]McVeigh, M. A., Grauer, W. K., and Paisley, D. J., "Rotor/Airframe Interactions on Tiltrotor Aircraft," 44th Annual Forum of the American Helicopter Society, June 1988.

[22]Weiberg, J. A., and Maisel, M., "Wind Tunnel Tests of the XV-15 Tilt Rotor Aircraft," NASA TM 81177, April 1980.

[23]Marcolini, M. A., Conner, D. A., Brieger, J. T., Becker, L. E., and Smith, C. E., "Noise Characteristics of a Model Tiltrotor," American Helicopter Society 51st Annual Forum and Technology Display, May 1995.

[24]Arrington, W. L., Kumpel, M., Marr, R. L., and McEntire, K. G., "Performance and Handling Qualities," *XV-15 Tilt Rotor Research Aircraft Flight Test Data Report*, Vol. 2, NASA CR 177406, 1985, pp. 7-1–9-390, Chaps. 7–9.

[25]Chehab, M., and Wolk, J., "A Windtunnel Study of X-Force Generators to Reduce Helicopter Blade–Vortex Interaction (BVI) Noise," 2000 AIAA Student Conf., April 2000.

[26]Burley, C. L., and Martin, R. M., "Tip-Path Plane Angle Effects on Rotor Blade–Vortex Interaction Noise Levels and Directivity," 44th Annual Forum of the American Helicopter Society, June 1988.

[27]Schmitz, F. H., and Sim, B. W.-C., "Radiation and Directionality Characteristics of Advancing Side Blade–Vortex Interaction (BVI) Noise," AIAA Paper 2000-1922, June 2000.

[28]Kitaplioglu, C., "Blade–Vortex Interaction Noise of a Full-Scale XV-15 Rotor Tested in the NASA Ames 80 by 120-Foot Wind Tunnel," NASA TM 1999-208789, July 1999.